Journal Name

ARTICLE TYPE

Cite this: DOI: 10.1039/xxxxxxxxxx

Anionic Order and Band Gap Engineering in Vacancy Ordered Triple Perovskites†

Taylor L. Hodgkins,[a] Christopher N. Savory,[b] Kelsey K. Bass,[a] Bethany L. Seckman,[a] David O. Scanlon,[bcd] Peter I. Djurovich,[a] Mark E. Thompson,[a] and Brent C. Melot[ad]

Received Date
Accepted Date

DOI: 10.1039/xxxxxxxxxx

www.rsc.org/journalname

We demonstrate that the optical absorption of the vacancy-ordered triple perovskite, $Cs_3Bi_2Br_9$, can be significantly red-shifted by substituting Br with I while maintaining the layered structural topology. We also present evidence that Br ions prefer to occupy the bridging halide position within the layers in order to minimize strain within the lattice that results from the incorporation of the significantly larger iodide anions into the lattice.

Perovskite $CH_3NH_3PbI_3$ and its structural derivatives have risen to prominence because of their promise as next-generation light absorbers in photovoltaic devices. Compared to existing technologies, their primary advantages lie in their high absorption coefficients, solution processability, and high carrier mobilities.[1–7] Yet with solar cells based on these materials now exceeding 22% efficiency, there has been a shift towards developing lead-free alternatives that will not pose as much risk of enviornmental contamination at end-of-life.[8,9]

The challenge in replacing Pb with chemically similar divalent metals is that elements like Sn and Ge are easily oxidized in air, which makes it challenging to maintain a uniform oxidation state, often producing heavily doped semiconductors.[10–12] In contrast, trivalent metals like Bi and Sb exhibit far superior oxidative stability but are incompatible with the traditional ABX_3 formulation of halide perovskites. Instead, these metals crystallize in analogous structures with the generic composition $A_3M_2X_9$, where a one-third vacancy on the metal site exists to maintain net charge neutrality.

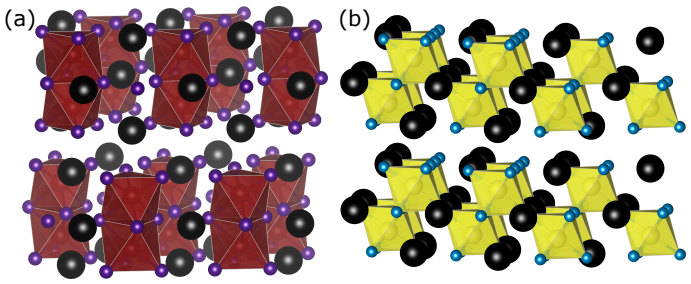

Fig. 1 Room temperature crystal structure of $Cs_3Bi_2Br_9$ and $Cs_3Bi_2I_9$. The dark grey atoms are Bi, light grey atoms are Br, light blue atoms are I, and black atoms are Cs.

To-date the most heavily explored member of this family has been $Cs_3Bi_2I_9$ because its 2 eV bandgap offers a fairly wide optical absorption window; however, all of the device work to-date has failed to exceed one percent efficiency.[13–15] Fundamentally, the poor charge collection seen for $Cs_3Bi_2I_9$ can be attributed to its zero-dimensional topology, as seen in Fig. 1 (a), which consists of face-sharing dimers of octahedra that are not directly connected to one another.[16] This isolation weakens the extent of metal-ligand rehybridization and significantly reduces the carrier mobility throughout the material.[17] So despite the narrow bandgap, most of the photo-generated charge seems to remain trapped on the Bi_2I_9 dimers rather than being collected as photocurrent.[17]

Unlike the iodide analogue, $Cs_3Bi_2Br_9$ exhibits a two dimensional topology consisting of corrugated layers of perovskite-like corner-sharing octahedra as illustrated in Fig. 1 (b).[18] The difference between the two polymorphs is created by rearranging the vacancy order within the $A_3B_3X_9$ parent as illustrated in Supporting Information Fig. S-1. Yet, despite the enhanced metal-halide connectivity in the layered structure, the reduced covalent character within the bromide creates a wide band gap of 2.7 eV that restricts the photons that can be absorbed to the blue and ultraviolet parts of the solar spectrum.[18]

[a] *Department of Chemistry, University of Southern California, Los Angeles, CA 90089, USA E-mail: melot@usc.edu*
[b] *Department of Chemistry, University College London, Christopher Ingold Building, London WC1H 0AJ, United Kingdom*
[c] *Diamond Light Source Ltd., Diamond House, Harwell Science and Innovation Campus, Didcot, Oxfordshire OX11 0DE, United Kingdom*
[d] *Thomas Young Centre, University College London, Gower Street, London WC1E 6BT, United Kingdom*

† Electronic Supplementary Information (ESI) available: [details of any supplementary information available should be included here]. See DOI: 10.1039/b000000x/

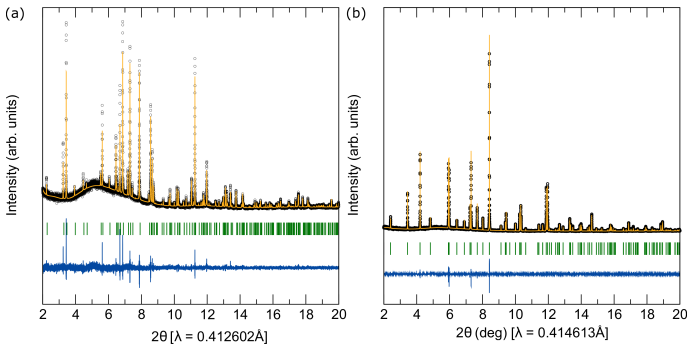

Fig. 2 Results of the Rietveld refinement of the (a) $Cs_3Bi_2I_9$ (χ^2 = 1.00) and (b) $Cs_3Bi_2Br_9$ (χ^2 = 1.51) structures against synchrotron X-ray diffraction patterns.

Here we have attempted to marry the narrower band gap of the iodide to the layered structure of the bromide by studying the effects of iodide substitution on the nuclear and electronic structure of $Cs_3Bi_2Br_{9-x}I_x$. In the process, we have found the layered topology of $Cs_3Bi_2Br_9$ is highly robust towards iodide substitution and is fully retained up to a maximum composition of $Cs_3Bi_2Br_3I_6$, above which phase-pure samples could not be obtained. Using high resolution synchrotron diffraction in combination with density functional theory calculations, we show evidence for segregation of the bromide and iodide anions within the mixed phases, which represents a rare example of anionic order in the halide perovskites. We also demonstrate that the band gap of the layered polymorph can be shifted nearly 700 meV from that of the pure bromide to become nearly identical to the pure iodide phase without distorting into the dimerized structure.

Figure 2 shows the results of Rietveld refinements of the iodide [Figure 2 (a)] and bromide [Figure 2 (b)] end members against the synchrotron X-ray diffraction patterns. Here, its clear that the hexagonal $P63/mmc$ structure of $Cs_3Bi_2I_9$ is easily distinguished from the $P3m1$ structure of $Cs_3Bi_2Br_9$. The diffusive hump in the background of the diffraction patterns corresponds to scattering from the kapton capillary sample holder, and is observable in all samples due to the requirement to dilute the samples in a matrix of fumed silica in order to reduce X-ray absorption from the heavy elements in the compounds. Full results for the refinements of the individual compositions can be found in Supporting Information Figs. S2-S8 and Tables S1-S7. As seen in Figure 4 (a), increasing substitution of iodide causes a steady increase in the d-spacing associated with the (220)/(024), (021)/(003), and (011) reflections as mirrored in the steady increase of the lattice parameters shown in Figure 4 (b). Simultaneously the (220) and (024) as well as the (021) and (003) peaks begin to consolidate into a single reflection. This merging of the peaks is primarily due to an increase in width that is clearly noticeable even in the $Cs_3Bi_2Br_8I$ with the smallest substitution of iodide. A microstructural analysis of the fitted profile indicates the broadening is primarily driven by a contribution from strain rather than particle size, which should be expected due to the 12% mismatch between the ionic radius of Br (1.96Å) and I (2.20Å).[19]

A closer inspection of the structure for the layered polymorph reveals a single unique position for Bi within lattice, and two for the halide and A sites. The multiplicity of the two halide positions is split between one-third of the atoms laying within the plane of corner-sharing octahedra and the other two-thirds arranged on the top and bottom of the slabs as illustrated in Fig. 3. Notably, an accurate description of the experimental intensity seen in the diffraction patterns could only be modeled by carefully refining the halide distribution between these two sites with typical improvements in R_{Bragg} ranging from 2-4% when site mixing was

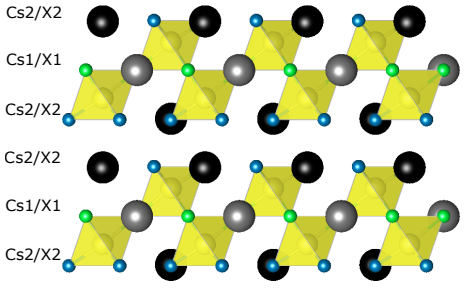

Fig. 3 View of the $Cs_3Bi_2Br_9$ structure with the splitting of the Cs and X sites explicitly labeled. Substituting iodide for bromide shows a clear preference for the $X2$ site over the $X1$, which is attributed to proximity to the Bi vacancy in the Van der Waals gap.

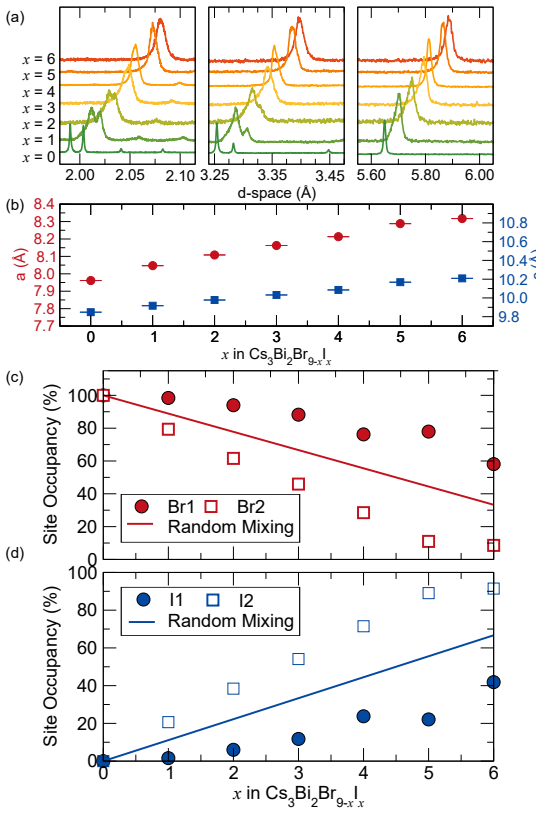

Fig. 4 (a) Selected reflections for the mixed halide phases showing that the trigonal structure of the bromide is maintained up until a composition of $Cs_3Bi_2Br_3I_6$. (b) Increase in the a and c lattice parameters as a function of iodide substitution. Distribution of (c) bromide and (d) iodide between the two sites as a function of nominal composition.

allowed. The lines shown in Figure 4 (c) and (d) delineate the ideal occupancy of each site given a random distribution based on the ideal composition; however, when the ratio of I and Br on each site was allowed to refine while maintaining the overall stoichiometry a clear partitioning of the I towards the site on top and bottom of the layer is found. Considering that this site is in proximity to the Bi vacancy, the iodide ions apparently localize to this position in order to alleviate the strain of the size mismatch. This would also appear to provide some insight into why single phase samples could only be obtained to a maximum of two-thirds iodide content, at which point iodide ions can no longer segregate to the gap and disfavor the interlayer position so much that the structure is unstable beyond this point.

The optical properties of the solid solution are shown in Fig. 5 with panel (a) isolating the end members and panel (b) showing the mixed halide phases. As has been previously reported, $Cs_3Bi_2I_9$ shows the shallow rise in absorption typically associated with an indirect band gap[20] whereas the $Cs_3Bi_2Br_9$ shows a steeper climb due to the small separation between the lowest lying indirect and a slighly higher direct absorption process. The mixed halide phases show a marked decrease in the band gap of over 300 meV in the x=1 which is then followed by the same steady trend seen earlier in the lattice parameters. Interestingly, the gap of $Cs_3Bi_2Br_3I_6$ (2.05 eV) appears to become nearly identical from that of the $Cs_3Bi_2I_9$ (2.06 eV) end member despite exhibiting the trigonal structure of the bromide phase.

To further explore changes in the chemical bonding across the solid solution, DFT calculations were performed to characterize changes in the electronic structure of the materials [Fig. 6 (a)-(c)]. Calculation of all possible substituted polymorphs allows us to assess the energetic penalty associated with substituting an iodine on a particular site. Across all substitutions, the lowest energy structures saw substitution at the vacancy-terminating

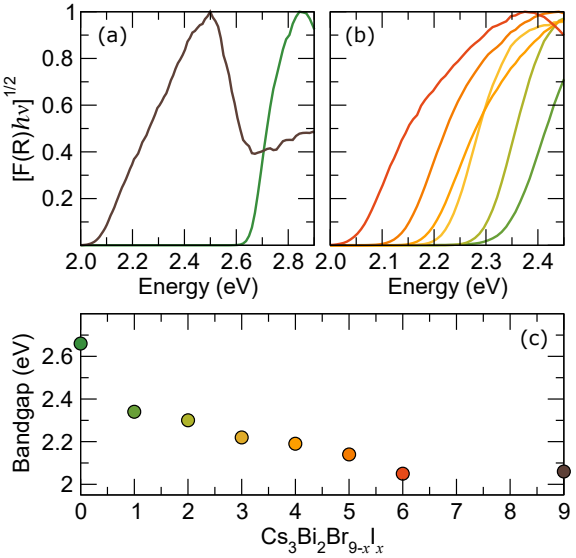

Fig. 5 Diffuse reflectance of the (a) end members and (b) mixed halide phases. (c) Band gap as determined by a linear fit to the onset of optical absorption.

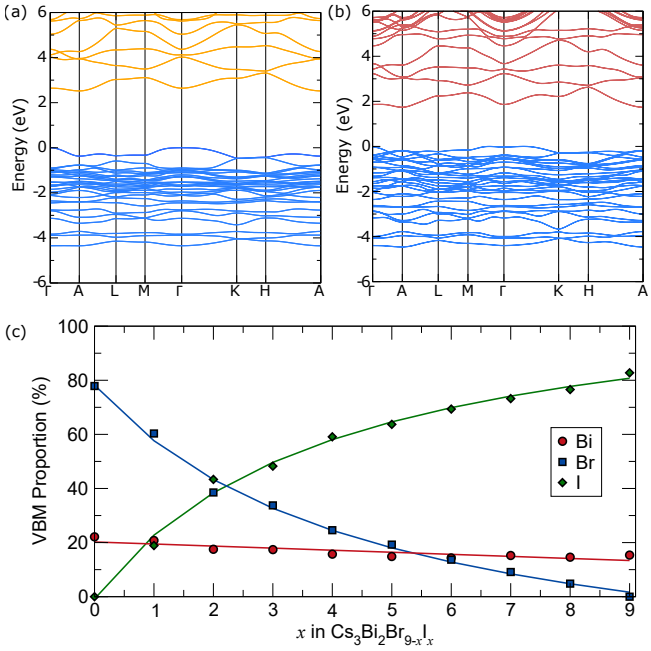

Fig. 6 Band structure of (a) $Cs_3Bi_2Br_9$ and (b) $Cs_3Bi_2I_9$ in the trigonal $P3m1$ layered polymorph. (c) Projected elemental composition of the valence band maximum as a function of iodine substitution. The solid lines are guides for the eye.

halide positions before the corner-sharing positions, indeed all polymorphs where a corner-shared halide was substituted were observed to be >40 meV per formula unit higher in energy than structures where a vacancy-terminated halide was substituted instead. The lowest energy structures also showed a consistent substitution pattern across the $Cs_3Bi_2Br_{9-x}I_x$ series wherein two vacancy-terminated halides are substituted on the same face of the Bi/Br layer, followed by two on the other face to relieve strain, and then the remaining vacancy-terminated halide positions before any of the corner-shared halides. Overall, these calculations appear to support a thermodynamic driving force behind the distribution of substituted sites seen in the refinements above. The calculated electronic structures of the substituted phases also show a monotonic decrease in the band gap as more iodine is substituted into the structure.

Projection of the atomic orbital character onto the bands shows that the top of the valence band for the substituted compounds consists of Bi-s, I-p, and Br-p orbitals with the percentage of I-p character increasing by 5-25% per substitution, while only altering the Bi-s character by 1-3% (Fig. 6 (c)). This is consistent with the ionization potential of the iodide states sitting slightly higher in energy than bromide, which results in a narrowing of the band gap with increasing iodide content as well as the unchanged shape of the conduction band minimum in the layered form of both the iodide and bromide, while there are clear differences in the valence band maxima [Figs. 6 (a) and (b)]. One can also clearly see an increase in the density of states at the top of the valence band, which may promote increased carrier conductivity when properly doped.

In conclusion, we have presented an optical and structural study of the $Cs_3Bi_2Br_{9-x}I_x$ solid solution and find the layered topology of the trigonal bromide structure can be maintained up to a maximum composition of $x=6$. By substituting iodide with bromide, the bandgap can be decreased from 2.66 eV to 2.05 eV for $Cs_3Bi_2Br_3I_6$, which is effectively identical to the hexagonal dimerized form of $Cs_3Bi_2I_9$. There are ongoing efforts to spin-cast films of this series since it has been challenging to obtain single phase films. These results provide insight into the crystal chemical origin of the zero-dimensional character of the $Cs_3Bi_2I_9$ end member and an avenue through which the carrier mobility of these fully inorganic solution processable semiconductors ocan be enhanced.

The experimental work shown here was partially supported by the Research Corporation for Science Advancement through a Cottrell Scholar to B.C.M. Computational work in this article used the UCL Legion and Grace HPC facilities (Legion@UCL and Grace@UCL) and the Archer UK National Supercomputing Service, which was accessed through the UK's HEC Materials Chemistry Consortium, funded by EPSRC (EP/L000202). CNS is grateful to the EPSRC and the Department of Chemistry at UCL for the provision of a DTA studentship (ref No. 1492829). D.O.S. acknowledges support from the European Research Council (grant no. 758345).

Conflicts of interest

There are no conflicts to declare.

Notes and references

1 W. Nie, H. Tsai, R. Asadpour, J.-C. Blancon, A. J. Neukirch, G. Gupta, J. J. Crochet, M. Chhowalla, S. Tretiak, M. A. Alam, H.-L. Wang and A. D. Mohite, *Science (New York, N.Y.)*, 2015, **347**, 522–5.
2 G. E. Eperon, V. M. Burlakov, P. Docampo, A. Goriely and H. J. Snaith, *Advanced Functional Materials*, 2014, **24**, 151–157.
3 P.-W. Liang, C.-Y. Liao, C.-C. Chueh, F. Zuo, S. T. Williams, X.-K. Xin, J. Lin and A. K.-Y. Jen, *Advanced Materials*, 2014, **26**, 3748–3754.
4 S. Sun, T. Salim, N. Mathews, M. Duchamp, C. Boothroyd, G. Xing, T. C. Sum and Y. M. Lam, *Energy Environ. Sci.*, 2014, **7**, 399–407.
5 D. Bryant, P. Greenwood, J. Troughton, M. Wijdekop, M. Carnie, M. Davies, K. Wojciechowski, H. J. Snaith, T. Watson and D. Worsley, *Advanced Materials*, 2014, **26**, 7499–7504.
6 F. Hao, C. C. Stoumpos, D. H. Cao, R. P. H. Chang and M. G. Kanatzidis, *Nature Photonics*, 2014, **8**, 489–494.
7 N. J. Jeon, J. H. Noh, Y. C. Kim, W. S. Yang, S. Ryu and S. I. Seok, *Nature Materials*, 2014, **13**, 897–903.
8 S. C. N. S. D. O. Ganose, A. M., *Chemical Communications*, 2017, **53**, 20–44.
9 J. M. Kadro and A. Hagfeldt, *Joule*, 2017, **1**, 29 – 46.
10 M. Konstantakou and T. Stergiopoulos, *Journal of Materials Chemistry A*, 2017, **5**, 11518–11549.
11 I. Kopacic, B. Friesenbichler, S. F. Hoefler, B. Kunert, H. Plank, T. Rath and G. Trimmel, *ACS Applied Energy Materials*, 2018, **1**, 343–347.
12 L.-J. Chen, *RSC Advances*, 2018, **8**, 18396–18399.
13 B. Ghosh, S. Chakraborty, H. Wei, C. Guet, S. Li, S. Mhaisalkar and N. Mathews, *The Journal of Physical Chemistry C*, 2017, **121**, 17062–17067.
14 B. Ghosh, B. Wu, H. K. Mulmudi, C. Guet, K. Weber, T. C. Sum, S. G. Mhaisalkar and N. Mathews, *ACS Applied Materials & Interfaces*, 2018, acsami.7b14735.
15 N.-G. Park, *Materials Today*, 2015, **18**, 65–72.
16 A. Nystrom and O. Lindqvist, *Acta Chemica Scandinavica*, 1967, **21**, 2570–2571.
17 M. W. W. J. M. D. B. a. Y. Y. Xiao, Z., *Materials Horizons*, 2017, **4**, 206–216.
18 K. K. Bass, L. Estergreen, C. N. Savory, J. Buckeridge, D. O. Scanlon, P. I. Djurovich, S. E. Bradforth, M. E. Thompson and B. C. Melot, *Inorganic Chemistry*, 2016, acs.inorgchem.6b01571.
19 R. D. Shannon, *Acta Cryst.*, 1976, **A32**, 751–767.
20 S. C. C. K. S. S. K. M. G. W. B. W. McCall, K. M., *Chemistry of Materials*, 2017, **29**, 4129–4145.